Proceedings of the IASTED International Conference
CIRCUITS, SIGNALS, AND SYSTEMS
November 28 - December 1, 2004, Clearwater Beach, FL, USA

RAPID STEADY-STATE ANALYSIS OF CLL RESONANT POWER CONVERTERS

†C. Gould, C. M. Bingham, D. A. Stone, M. P. Foster

Department of Electronic and Electrical Engineering
University of Sheffield, Mappin Street, Sheffield, S1 3JD, UK
Tel. +44 (0) 114 2225847, Fax. +44 (0) 114 2225196
†Corresponding author: e-mail: elp02crg@sheffield.ac.uk

ABSTRACT
Cyclic averaging techniques are applied to the CLL resonant power converter to provide steady-state converter characteristics for rapid stress analysis. This is shown to facilitate the determination of mode duties and initial conditions through knowledge of the operational modes of the rectifier at various operating frequencies. Comparisons are made with FMA-based cyclic analyses, and Spice simulations, that show, respectively, improved accuracy and vastly improved execution speeds.

KEY WORDS
Resonant power converters, Cyclic analysis

1. Introduction
Resonant power converters are attracting a resurgence of interest for the development of efficient DC-DC power supplies. This is primarily due to the inherent 'soft-switching' action that facilitates the use of higher excitation frequencies, resulting in a desirable downsizing of reactive components. Of the many 3-element resonant topologies [1-3], the split-inductor arrangement of the CLL converter (shown in Fig. 1) is of particular interest, since it can utilise parasitic elements inherent in isolation transformers (necessary for safety in commercial products), thereby allowing high-order topologies to be realised for applications such as airborne radar, flat screen televisions and distributed power supplies. These high-order resonant systems are, however, highly non-linear, which complicates their analysis and design.

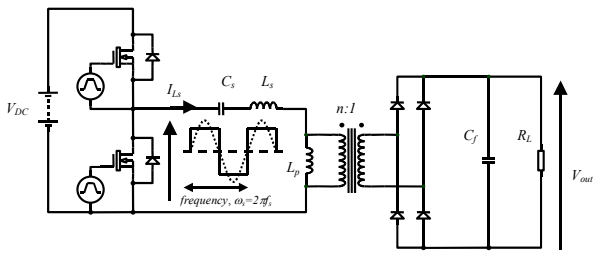

Fig. 1. Voltage-output CLL resonant converter topology

An important property of the CLL resonant converter is that it can benefit from an almost load independent design point (positioned at the tank series-resonant frequency) that is above the system resonant frequency [2], thereby allowing classical inductive (Zero-Voltage) switching characteristics over the full load range. This combined with low turn-off current in the MOSFETs (thereby facilitating low-loss switching) make the CLL converter an attractive choice for efficient, compact power supplies.

2. Analysis of Resonant Converters
Traditionally, resonant converters are analysed through the use of Fundamental Mode Approximation (FMA) [1, 6-8] or variants thereof [9-11], as well as other frequency-domain techniques, all of which can predict the behaviour of the converter to a degree of accuracy dictated by assumptions made during modelling. State-variable techniques can also be utilised to provide very accurate transient time-domain solutions [12-14], through the use of integration-based simulation packages. However, the reliance on integration imparts significant computational overhead, and is therefore time consuming. Because of this, many authors have sought closed-form (steady-state) solutions of the piecewise linear state-variable equations. Such techniques, however, require *a priori* knowledge of the converters behaviour at each frequency - in particular, the type and number of modes of operation that exist in a cycle, and their duty. Whilst the latter can usually be approximated through FMA (or similar techniques), these often prove inaccurate and render undesirable analysis results (as will be demonstrated). Other authors [15-16] have overcome the need for *a priori* knowledge through the utilisation of Chebyshev polynomial approximations and initial guesses for the mode duties (i.e. Newton's algorithm for convergence), thereby achieving useful transient analyses of switched circuits; though incurring iterative loops in the algorithm.
In [17], an accurate 'initial guess' and robust algorithm is proposed that utilises interval analysis and the compensation theorem. Again, fast and accurate transient analyses for regulated DC-DC converters, is shown, though with the drawback of requiring iterative search methods and additional memory requirements (to store correctly identified mode descriptions).
If only steady state waveforms are required, i.e. for use in a Graphical User Interface (GUI) for accurate, rapid stress analysis of converter designs, cyclic-averaging techniques [18] can be applied to resonant converters [11, 19] that provide analytical time-domain solutions for the converter's internal voltages and currents. Given *a priori* knowledge of the mode-order and, most importantly, the length of each duty, these techniques are demonstrated to be of comparable accuracy to Spice whilst requiring only a small fraction (typically 1/10,000th) of the execution

time. In [11, 19], the mode duties are calculated using FMA or modified FMA techniques, and the corresponding accuracy of the output voltage in the frequency domain, is demonstrated. Here, the FMA estimations are verified in the time domain, and whilst output voltages are seen to be commensurate with results from Spice and practical converters, the accuracies of the current and voltage waveforms suffer.
Instead, therefore, it will be demonstrated that for particular converter topologies, the cyclic process itself can be utilised, in conjunction with basic network theory, to provide rapid and accurate analysis of the converters.

3.1. Cyclic Modelling Methodology

In steady-state, a converter is 'cyclic' when the state vector at the beginning of the switching period, $x(t)$, is equal to the state vector at the end of the switching period, $x(t + T)$. Or more generally:

$$x(t) = x(t + NT) \tag{1}$$

where T is the period of the input voltage and N is an integer number of cycles. During each cycle the converter can be divided into distinct operating modes, dictated by the state of the switches (i.e. polarity of input voltage) and circuit currents and voltages. Each of these modes can be described using a piecewise linear equations. In general, for the i^{th} operating mode:

$$\dot{x}(t) = A_i x(t) + B_i \tag{2}$$

where A_i is the dynamical system matrix of the i^{th} mode ($n \times n$), and B_i the mode's excitation matrix ($n \times 1$), and $i \in 1\ldots m$. Assuming that each cycle begins at time t_0, and ends at time t_m, where t_m-$t_0 = T$, the length of the i^{th} mode is given by $\Delta t_i = t_i$-$t_{i-1} = d_i T$, where d_i is a parameter known as the duty of the i^{th} mode. The sum of the m duties must equal unity for a complete cycle. From [18], the system can be solved to find the evolution of the state vector:

$$\begin{aligned} x(t_i) &= e^{A_i d_i T} x(t_{i-1}) + \int_{t_{i-1}}^{t_i} e^{A_i (t_i - \tau)} B_i \, d\tau \\ &= \Phi_i x(t_{i-1}) + \Gamma_i \end{aligned} \tag{3}$$

where: $\Phi_i = \Phi(t_i, t_{i-1}) = e^{A_i d_i T}$, $\Gamma_i = \int_{t_{i-1}}^{t_i} e^{A_i (t_i - \tau)} B_i \, d\tau$, and $x(t_i)$ are the initial conditions for the i^{th} mode. To simplify the analysis, an augmented state vector can be introduced by virtue of the piece-wise linear nature of the system:

$$\frac{d}{dt}\begin{pmatrix} x(t_i) \\ \hline 1 \end{pmatrix} = \left(\begin{array}{c|c} A_i & B_i \\ \hline 0 & 0 \end{array}\right)\begin{pmatrix} x(t_i) \\ \hline 1 \end{pmatrix} \tag{4}$$

or $\dfrac{d}{dt}\hat{x}(t_i) = \hat{A}_i \hat{x}(t_i)$

A solution of (4) is found by noting that the initial conditions for the $(i+1)^{th}$ mode are the results from the previous i^{th} mode:

$$\hat{x}(t_1) = e^{\hat{A}_i d_i T}\hat{x}(t_0) = \hat{\Phi}_1 \hat{x}(t_0) \tag{5}$$

$$\hat{x}(t_i) = e^{\hat{A}_i d_i T}\hat{x}(t_{i-1}) = \hat{\Phi}_i \hat{x}(t_{i-1}) \tag{6}$$

$$\hat{x}(t_m) = \hat{\Phi}_m \hat{\Phi}_{m-1} \cdots \hat{\Phi}_1 \hat{x}(t_0) = \hat{\Phi}_{tot} \hat{x}(t_0) \tag{7}$$

where, $\hat{\Phi}_i = \left(\begin{array}{c|c} \Phi_i & \Gamma_i \\ \hline 0 & 1 \end{array}\right)$ and $\hat{x}(t_m)$ is the state-vector at time t_m for an initial condition $\hat{x}(t_0)$. The cyclic solution for the initial condition, $\hat{x}_{per}(t_0)$, can be obtained by equating $\hat{x}(t_0)$ with $\hat{x}(t_m)$.

$$\therefore \quad x_{per}(t_0) = \left(I^n - \Phi_{tot}\right)^{-1} \Gamma_{tot} \tag{8}$$

3.2. Modelling of the voltage-output CLL converter

The converter is analysed by partitioning the dynamics into fast and slow sub-systems, related by coupling equations. For this converter topology, the fast sub-system includes the action of the power switches and resonant circuit, whilst the slow system consists of the output filter. A coupling equation relates the highly non-linear behaviour of the rectifier to the fast and slow dynamics.
Fig. 2 shows the converter in terms of its idealised reactive components and associated parasitic resistances, and an equivalent model of the bridge rectifier during Continuous Conduction Mode (CCM), comprising of diode on-state voltages, V_d, and resistances r_f. The MOSFET drain-source resistance during conduction is modelled by r_{ds}. To avoid undue complication, the transformer shown in Fig. 1 is assumed to have a 1:1 turns ratio, and is therefore modelled, as in Fig. 2, solely by its magnetising inductance, L_p, and winding resistance, r_{Lp}.

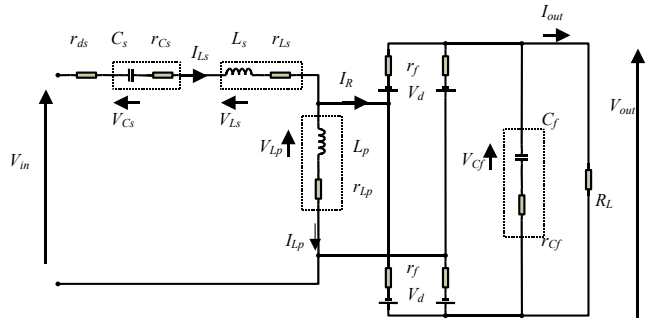

Fig. 2. State-variables of CLL converter (voltage-output)

Utilising basic network theory the converter can be described by:

$$\begin{bmatrix} \dot{I}_{L_p} \\ \dot{V}_{C_s} \\ \dot{I}_{L_s} \\ \dot{V}_{C_f} \end{bmatrix} = \begin{bmatrix} \frac{-R_{op}\cdot r_{C_f} - 2r_f - r_{L_p}}{L_p} & 0 & \frac{R_{op}\cdot r_{C_f} + 2r_f}{L_p} & \mathrm{sgn}(I_R)\cdot\frac{R_{op}}{L_p} \\ 0 & 0 & \frac{1}{C_s} & 0 \\ \frac{R_{op}\cdot r_{C_f} + 2r_f}{L_s} & \frac{-1}{L_s} & \frac{-R_{op}\cdot r_{C_f} - 2r_f - r}{L_s} & -\mathrm{sgn}(I_R)\cdot\frac{R_{op}}{L_s} \\ -\mathrm{sgn}(I_R)\cdot\frac{R_{op}}{C_f} & 0 & \mathrm{sgn}(I_R)\cdot\frac{R_{op}}{C_f} & \frac{-R_{op}}{C_f\cdot R_L} \end{bmatrix} \cdot \begin{bmatrix} I_{L_p} \\ V_{C_s} \\ I_{L_s} \\ V_{C_f} \end{bmatrix} + \begin{bmatrix} \mathrm{sgn}(I_R)\cdot\frac{2V_d}{L_p} \\ 0 \\ \frac{V_{in} - \mathrm{sgn}(I_R)\cdot 2V_d}{L_s} \\ 0 \end{bmatrix} \quad (9)$$

where : $Rop = \frac{R_L}{R_L + r_{C_f}}$ and $r = r_{ds} + r_{C_s} + r_{L_s}$

In this case, the only variables in the system are the polarities of the input voltage and rectifier current. Since these can each be in one of two states (for operation in continuous conduction mode), this totals four modes of operation (see Fig. 3).

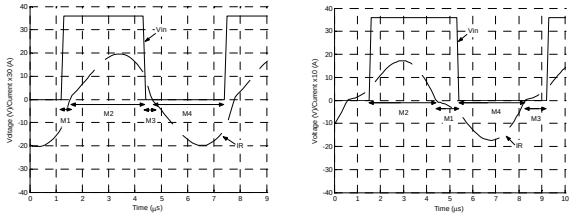

(a) (b)

Fig. 3. Cyclic modes of CLL converter (a) above series resonance (160kHz), and (b) below series resonance (130kHz)

Normal operation will be considered to occur at, or above, the series resonant frequency. Hence, given that a positive input voltage transition marks the start of a cycle, convention for mode description becomes:

Mode 1: $V_{in} = V_{DC}$, and $I_R < 0$ hence $sgn(I_R) = -1$
Mode 2: $V_{in} = V_{DC}$, and $I_R > 0$ hence $sgn(I_R) = 1$
Mode 3: $V_{in} = 0$, and $I_R > 0$ hence $sgn(I_R) = 1$
Mode 4: $V_{in} = 0$, and $I_R < 0$ hence $sgn(I_R) = -1$

3.3. Determination of duties

Accurate knowledge of mode duties is crucial for correct determination of the converter's initial conditions and behaviour. FMA techniques established in [8] are initially used to provide estimates of the mode lengths, and their performance at predicting waveforms, is assessed.

3.3.1. FMA estimation of first mode

From [8] the phase-angle between the input voltage and rectifier current can be found from:

$$\varphi = \tan^{-1}\left\{\frac{\frac{1}{Q_L}\cdot\left(\frac{\omega_s}{\omega_0}\cdot\frac{A}{A+1} - \frac{\omega_0}{\omega_s}\right)}{(1+A)\cdot\left[1-\left(\frac{\omega_0}{\omega_s}\right)^2\right]}\right\} \quad (10)$$

where: $A = L_s/L_p$, ω_o = fundamental frequency, ω_s = switching frequency, and Q_L = loaded quality factor at ω_o. The duty for the first mode is found by normalising with respect to 2π, and the subsequent duties found by symmetry. However, for operation below the series resonance, the angle obtained can be negative (since the rectifier can switch capacitively, hence, the rectifier current leads the input voltage, as shown in Fig. 3(b)). In this case the modes operate in an alternative sequence (if the positive input voltage transition still marks the beginning of a cycle). The first duty is then found through subtracting the magnitude of the normalized angle from 0.5. Subsequent modes can again be found through symmetry.

Since Zero Voltage Switching (ZVS) is required for efficient operation, predictions must be limited to frequencies above the system resonance (ω_r). Therefore, the duties may be described more generally by:

$$d_1 = \begin{cases} \frac{1}{2\pi}\tan^{-1}\left\{\frac{\frac{1}{Q_L}\cdot\left(\frac{\omega_s}{\omega_0}\cdot\frac{A}{A+1} - \frac{\omega_0}{\omega_s}\right)}{(1+A)\cdot\left[1-\left(\frac{\omega_0}{\omega_s}\right)^2\right]}\right\} & \text{for} \left(\frac{\omega_s}{\omega_o}\right) \geq \sqrt{1+\frac{1}{A}} \\ 0.5 + \frac{1}{2\pi}\tan^{-1}\left\{\frac{\frac{1}{Q_L}\cdot\left(\frac{\omega_s}{\omega_0}\cdot\frac{A}{A+1} - \frac{\omega_0}{\omega_s}\right)}{(1+A)\cdot\left[1-\left(\frac{\omega_0}{\omega_s}\right)^2\right]}\right\} & \text{for} \left(\frac{\omega_r}{\omega_o}\right) < \left(\frac{\omega_s}{\omega_o}\right) < \sqrt{1+\frac{1}{A}} \end{cases}$$

$$d_2 = 0.5 - d_1 \quad (11)$$
$$d_3 = d_1$$
$$d_4 = d$$

An example converter (r_{ds} =0.19Ω, C_s =23nF, r_{Cs} =46mΩ, L_s =54.3µH, r_{Ls} =0.7Ω, L_p =29.9µH, r_{Lp} =0.7Ω, V_d =0.8V, r_f =1Ω, C_f =100µF, r_{Cf} =0.44Ω, R_L =20Ω, resonant frequency f_r =128kHz) is used to provide a demonstration of model accuracy. From practical measurements using sub-series resonant switching (130kHz), and supra-series resonant switching (160kHz), the converter can be seen to possess waveforms shown below in Fig. 4. By inspection, a duty of 0.04 (or 4% of the time-period of operation) can be seen to develop an average output voltage of 8.77V for 160kHz operation, whilst 130kHz operation yields 17.8V with a duty of 0.372 (37.2%).

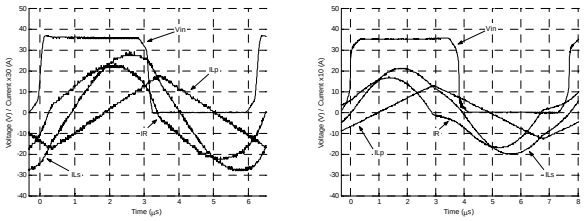

(a) (b)

Fig. 4. Practical waveforms of converter operated at (a) 160kHz and (b) 130kHz

FMA estimates of the duties produce 3.5% difference compared to practical results for 160kHz operation, and 1.5% difference at 130kHz. Subsequent application of the cyclic analysis at these frequencies yields 20.6% error in the average output voltage for 160kHz operation and a 16.7% error for 130kHz. Conversely, Spice simulation of the converter at 160kHz produces 5.8% output voltage error for a 1.4% duty error, and 16.7% output voltage error for 8.7% duty error at 130kHz operation. The waveforms generated by both modelling methods are shown in Fig. 5.

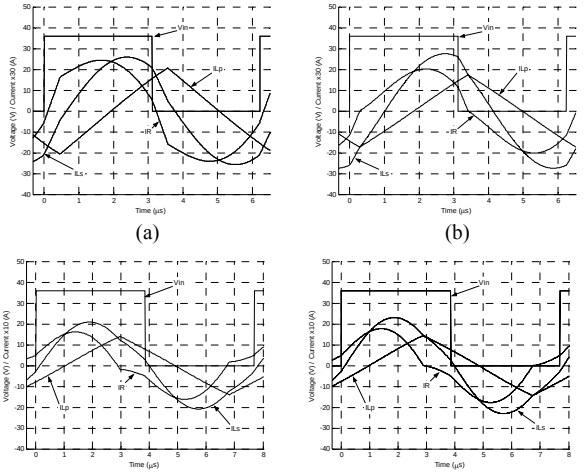

(a) (b) (c) (d)

Fig. 5. Circuit currents referred to input voltage from (a) FMA cyclic predictions at 160kHz, (b) Spice predictions for operation at 160kHz, (c) FMA cyclic predictions at 130kHz and (d) Spice predictions for operation at 130kHz

It is evident from Fig. 5 that large errors between the duties can have a significant effect on the accuracy of the initial conditions and resulting waveforms, and hence, the accuracy of the output voltage predictions. Yet it is shown that with greater accuracy in the calculation of the first duty, the prediction of output voltage approaches that of the presented converter.

From an execution speed perspective, the FMA-based cyclic predictions take ~0.14 seconds (with step sizes of 10 nanoseconds) compared to ~730 seconds for the Spice transient analysis (10ms to steady state) with same step-size.

3.3.2. Numeric search from a FMA initial condition

Improvement of the duty accuracy can be obtained by noting that the first mode must end as I_{L_s} becomes equal to I_{L_p} (since $I_R = 0$), when i_{L_p} changes polarity. By iteratively sweeping the duty from the initial FMA prediction towards 0 or 0.5, the correct duty can be found when the cyclic analysis correctly predicts the two boundary conditions. By way of example, Fig. 5(a) shows the discrepancy produced when the duty is incorrect. It can be seen that I_{L_s} becomes equal to I_{L_p} some time before i_{L_p} changes polarity.

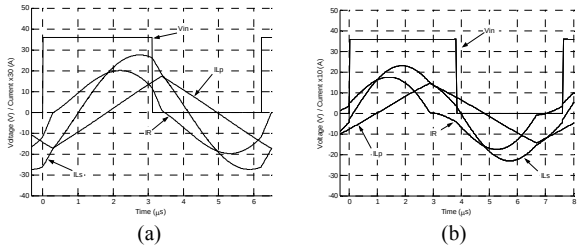

(a) (b)

Fig. 6. Circuit currents referred to input voltage from iterative cyclic predictions for (a) operation at 160kHz, and (b) 130kHz.

Conversely, Fig. 6 highlights the improvements due to the iteration at both operating frequencies, with a much higher correlation between the cyclic and Spice predictions being evident. Specifically, at 160kHz a duty error of 0.8% produces an output voltage error of 0.8%. Notably, the execution time has increased to 1/250th (2.93 seconds) of that for the generation of 'equivalent' Spice results. Likewise, for 130kHz operation the errors are 0.6% (duty) and 1.3% (output voltage) with an execution time of 1/175th (2.04 seconds) compared to Spice.

3.3.4. Cyclic estimation

The two techniques shown above demonstrate the need for an equation-based, current-bounded technique for fast, accurate estimation of d_1. Through modifications to the scheme presented for finding the initial conditions of a cyclic system (8), it can be shown that cyclic analysis can be employed to provide accurate estimations of the first duty.

By describing the input voltage as a bipolar square wave, the fast and slow sub-systems become anti-symmetrical and the initial conditions can be obtained from just 2 modes, requiring only that the identity matrix in (8) be replaced with the modified matrix:

$$C = \begin{bmatrix} -1 & 0 & 0 & 0 \\ 0 & -1 & 0 & 0 \\ 0 & 0 & -1 & 0 \\ 0 & 0 & 0 & 1 \end{bmatrix} \tag{12}$$

(describing the polarity of the fast and slow sub-systems).

Consider the new conventions for describing the modes in Fig. 7—each half-cycle now begins in M2 for supra-series resonant switching, and M1 for sub-series resonant operation. Since $I_R = 0$ at the start and finish of each half-cycle for both forms of switching, the vector of initial conditions obtained will contain equal values for I_{L_p} and I_{L_s} since $I_R = I_{L_s} - I_{L_p}$. Knowing that these values must be equal, the cyclic process can be performed with the time-period of operation (T) and the duty d_3 (for supra-series resonant switching or d_4 for sub-series resonant switching) set as an algebraic variable—the resulting vector of initial conditions thereby containing values of I_{L_p} and I_{L_s} in terms of T and d_3 (or d_4), that can be equated, and solved for a given frequency of operation. Symmetry then allows the calculation of other modes.

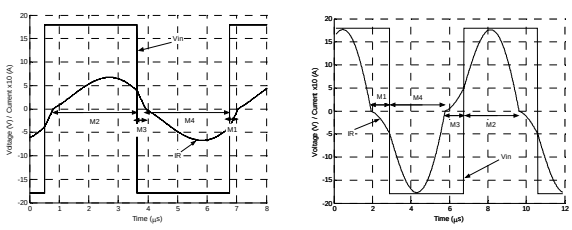

(a) (b)

Fig. 7. Modified cyclic modes for (a) supra-series resonance operation and (b) sub-series resonance operation

Using only 2 modes, the system can be described by:

$$\hat{x}(t_m) = \hat{\Phi}_3 \hat{\Phi}_2 \hat{x}(t_0) = \hat{\Phi}_{tot} \hat{x}(t_0) \quad (13)$$

(for supra-series resonance switching)

$$\hat{x}(t_m) = \hat{\Phi}_4 \hat{\Phi}_1 \hat{x}(t_0) = \hat{\Phi}_{tot} \hat{x}(t_0) \quad (14)$$

(for sub-series resonance switching)

where: $\hat{\Phi}_1 = e^{\hat{A}_1(0.5-d_4)T}$, $\hat{\Phi}_2 = e^{\hat{A}_2(0.5-d_3)T}$, $\hat{\Phi}_3 = e^{\hat{A}_3 d_3 T}$ and $\hat{\Phi}_4 = e^{\hat{A}_4 d_4 T}$.

The exponentials are evaluated algebraically through use of binomial expansions and '*p*' elements of the Taylor series:

$$e^{\hat{A}_i(0.5-d_j)T} = \sum_{p=0}^{p=\infty} \frac{\hat{A}_i^{\,p} T^p}{p!} \cdot \sum_{k=0}^{p} \binom{p}{k} 0.5^{p-k} (-d_j)^k \quad (15)$$

(for i=1, j=4 and i=2, j=3)

$$e^{\hat{A}_i d_i T} = \sum_{p=0}^{p=\infty} \frac{\hat{A}_i^{\,p} \cdot (d_i T)^p}{p!} \quad (16)$$

(for i=3 and i=4)

From (15) and (16), it is evident that for high values of p, high powers of d_3 or d_4 will be present in the algebraic solution of each exponential, thus complicating the total solution process, whilst small values of p will introduce errors into the solution for the mode duties. Since the error incurred when using p elements of the Taylor series is:

$$E(p) = \sum_{q=p+1}^{q=\infty} \frac{\hat{A}_i^{\,q} \cdot (d_i T)^q}{q!} \quad (17)$$

the greatest error naturally occurs when the product $(d_i \cdot T)$ is largest, which for any frequency occurs just before the series-resonant frequency (i.e. when the first mode duty approaches 0.5).

Using knowledge of the resonant frequency to obtain the largest ZVS value for T, Fig. 8 shows the correlation between the number of elements of the Taylor series, and the maximum error in the calculation of any term in the numerical matrix exponential.

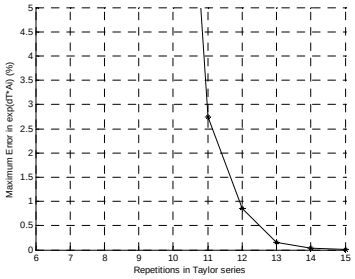

Fig. 8. Effect of number of terms used in Taylor series on maximum error in numerical matrix exponential

Evidently, for this particular converter, it is safe to assume that 12 elements of the Taylor series are adequate to produce less than 1% error in any of the matrix exponential terms, thereby resulting in a reliable value for the first mode duty.

Using common mathematical software packages (eg. Maple or Symbolic Matlab), (13) and (14) can be solved using the exponential descriptions in (15) and (16). The resulting algebraic vector for the initial conditions will therefore contain the values for I_{L_s} and I_{L_p} when $I_R = 0$, which are then equated and ordered into a 96th order polynomial (since 12 elements are used in the Taylor series). A software package is then used to find the 96 roots of the polynomial and the single real root existing in the range 0 → 0.5 (i.e. a half-cycle of operation), representing d_3 (or d_4) can be obtained. A definitive theorem showing that only a single real-solution exists in the range 0 → 0.5 has not yet been forthcoming. However, a sample of 100 CLL converter designs with specifications randomly taken from the following ranges: Output power = 100W → 1kW, output current = 1A → 10A, fundamental frequency = 50kHz → 150kHz, Switching frequency = 50kHz → 1.5MHz, parallel inductor = 10μH → 1mH, all parasitics = 5mΩ → 1Ω, have been simulated to steady-state using Spice, and the duty d_1 subsequently obtained. Estimates of d_1 of the 100 designs, using the proposed cyclic-estimation method, showed that all solutions resulted in a single real root in the range 0 → 0.5, and the % difference between the Spice results and the estimates, shown in Fig. 9, confirms that excellent accuracy is obtained.

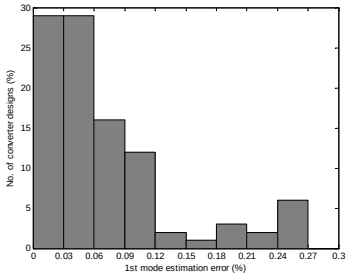

Fig. 9. Percentage difference between cyclic and Spice models for estimation of 1st mode duty.

Application of the cyclic estimation technique to the original converter described previously results in the waveforms shown in Fig. 10, for both 160kHz and 130kHz operation.

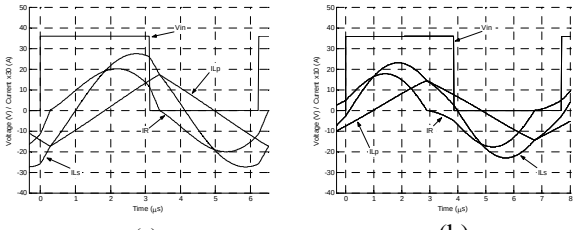

(a) (b)

Fig. 10. Circuit currents referred to input voltage from cyclic predictions with cyclic 1st mode estimation for (a) operation at 160kHz, and (b) 130kHz.

The cyclic estimation of the first duty produces a 0.6% error for 160kHz, and 0.4% error for 130kHz operation. From an output voltage perspective, the cyclic estimation produces errors of 1.8% and 2.2% for 160kHz and

130kHz operation, respectively, with execution times of approximately 1/3720th and 1/2830th of that required by Spice. The methodology is, therefore, demonstrated to operate with the same order of computation speed as that of FMA predicted cyclic analysis, yet with the equivalent accuracy of a numerical-search approach to calculating the duties. For completeness, Fig. 11 shows the resulting output voltage from the proposed cyclic estimation techniques, in the frequency domain, when compared to measurement taken from the presented experimental converter.

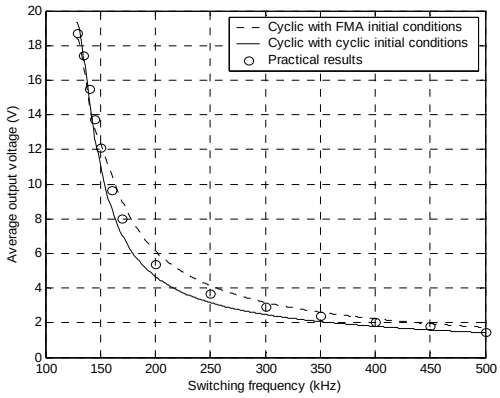

Fig. 11. Practical frequency response of converter with cyclic analyses using FMA and cyclic initial conditions

4. Conclusion

For analysis of the steady-state stresses on components in the converter, cyclic modelling techniques have been applied to provide fast and accurate steady-state time domain solutions. A new method for estimating the mode duties for Continuous Conduction Mode operation, has been proposed. The method relies on the currents in the series and parallel branches of the inverter being equal at the beginning and end of each cycle in steady-state. The method is shown to provide duties for a wide range of converters with accuracies of better than 99% when compared with both practical waveforms and transient Spice results (employed as the speed metric throughout the paper).

References:

[1] R. L. Steigerwald, A Comparison of Half-Bridge Resonant Converter Topologies, IEEE Trans. Power Electronics, April 1988. Vol. 3, no. 2, pp174-182

[2] R. P. Severns, Topologies for three element resonant converters, IEEE Trans. Power Electronics, Jan. 1992. Vol. 7, no. 1, pp 89-98

[3] I. Batarseh, Resonant Converter Topologies with Three and Four Energy Storage Elements, IEEE Trans. Power Electronics, Jan. 1994. Vol. 9, no. 1, pp 64-73

[4] B. Yang, R. Chen, F. C. Lee, Integrated Magnetic for LLC Resonant Converter, Seventeenth Annual IEEE Applied Power Electronics Conference and Exposition (APEC) 2002, pp 346-351

[5] A. Kats, G. Ivensky, Ben-Yaakov, Application of Integrated Magnetic in Resonant Converters, Twelfth Annual IEEE Applied Power Electronics Conference and Exposition (APEC) 1997, vol. 2, pp 925-930

[6] G. S. N. Raju, S. Doradla, An LCL resonant converter with PWM control-analysis, simulation, and implementation, IEEE Trans. Power Electronics, March 1995, vol. 10, no 2, pp 164-74

[7] A. K. S. Bhat, S. B. Dewan, Analysis and design of a high-frequency resonant converter using LCC-type commutation, IEEE Trans. Power Electronics, October 1987, vol. pe-2, no.4, pp 291-300

[8] M. K. Kazimierczuk, D. Czarkowski, Resonant Power Converters, Wiley, April 1995, pp 437-448

[9] J. G. Hayes, M. G. Egan, Rectifier-compensated Fundaments Mode Approximation Analysis of the series-parallel LCLC family of resonant converters with capacitive filter and voltage-source load, PESC'99 record 30th IEEE Power Electronics Specialist Conference, 1999, vol.2, pp1030-1036

[10] A. J. Forsyth, G. A. Ward, S. V. Mollov, Extended Fundamental Frequency Analysis of the LCC Resonant Converter, IEEE Trans. On Power Electronics, Nov. 2003, vol. 18 (6), pp1286-1292

[11] M. P. Foster, H. I. Sewell, C. M. Bingham, D. A. Stone, D. Hente, D. Howe, Cyclic-averaging for high-speed analysis of resonant converters, IEEE Trans. Power Electronics, July 2003, vol. 18 (4), pp985-993

[12] C. Gould, D. A. Stone, M. P. Foster, C. M. Bingham, State-variable Modelling of CLL Resonant Converters, Record: 2nd International IEE Power Electronics, Machines & Drives Conference, 2004, pp 214-219

[13] M. P. Foster, H. I. Sewell, C. M. Bingham, D. A. Stone, State-variable Modelling of LCC Voltage Output Converters, IEE Electronics Letters, 2001, (17), pp.1065-1066

[14] Y. Ang, M. P. Foster, H. I. Sewell, C. M. Bingham, D. A. Stone, Stress analysis of fourth-order LLCC resonant converters, IEE Electronics Letters, Nov. 2002, vol. 38 (24), pp1585-1586

[15] A. M. Luciano, A. G. M. Strollo, A Fast Time-Domain Algorithm for the Simulation of Switching Power Converters, IEEE Trans. Power Electronics, vol. 5 (3) July 1990, pp363-370

[16] K. K. Tse, H. S. Chung, S. Y. R. Hui, Stepwise Quadratic State-Space Modelling Technique for Simulation of Power Electronics Circuits, IEEE Trans. Industrial Electronics, vol. 46 (1) Feb 1999, pp91-99

[17] N. Femia, G. Spagnuolo, M. Vitelli, Steady-State Analysis of Hard and Soft Switching DC-to-DC Regulators, IEEE Trans. Power Electronics, vol. 18, (1), Jan 2003, pp51-64

[18] H. R. Visser, P. P. J. Van den Bosch, Modelling of Periodically Switching Networks, PESC 91 Record 22nd IEEE Power Electronics Specialist Conference, 1991, pp 67-73

[19] Y. Ang, M. P. Foster, C. M. Bingham, D. A. Stone, H. I. Sewell, D. Howe, Analysis of 4th-order LCLC Resonant Power Converters, IEE Proc: Electric Power Applications, March 2004, vol. 151, no. 02, pp 169-181